This loss of contrast is likely to be due to a relaxation of the level population during the measurement itself.

In order to understand what limits the coherence time of the circuit, measurements of the linewidth $\Delta\nu_{01}$ of the resonant peak as a function of $U$ and $\Phi$ have been performed. The linewidth increases linearly when departing from the optimal point ($N_g = 1/2$, $\phi = 0$, $I_b = 0$). This dependence is well accounted for by charge and phase noises with root mean square deviations $\Delta N_g = 0.004$ and $\Delta(\delta/2\pi) = 0.002$ during the time needed to record the resonance. The residual linewidth at the optimal working point is well explained by the second-order contribution of these noises. The amplitude of the charge noise is in agreement with measurements of $1/f$ charge noise (*31*), and its effect could be minimized by increasing the $E_J/E_{CP}$ ratio. The amplitude of the flux noise is unusually large (*32*) and should be significantly reduced by improved magnetic shielding. An improvement of $Q_\varphi$ by an order of magnitude thus seems possible. Experiments on quantum gates based on the controlled entanglement of several capacitively coupled quantronium circuits could already be performed with the level of quantum coherence achieved in the present experiment.

**References and Notes**


1. M. A. Nielsen, I. L. Chuang, *Quantum Computation and Quantum Information* (Cambridge Univ. Press, Cambridge, 2000).
2. *The Physics of Quantum Information: Quantum Cryptography, Quantum Teleportation, Quantum Computation*, D. Bouwmeester, A. Ekert, A. Zeilinger, Eds. (Springer-Verlag, Berlin, 2000).
3. V. B. Braginsky, F. Ya. Khalili, *Quantum Measurement* (Cambridge Univ. Press, 1992).
4. W. H. Zurek, J. P. Paz, in *Coherent Atomic Matter Waves*, R. Kaiser, C. Westbrook, F. David, Eds. (Springer-Verlag, Heidelberg, Germany, 2000).
5. P. W. Shor, *Phys. Rev. A* **52**, R2493 (1995).
6. A. M. Steane, *Phys. Rev. Lett.* **77**, 793 (1996); *Rep. Prog. Phys.* **61**, 117 (1998).
7. J. Preskill, *J. Proc. R. Soc. London Ser.* A **454**, 385 (1998)
8. Y. Makhlin, G. Schön, A. Shnirman, *Rev. Mod. Phys.* **73**, 357 (2001).
9. M. H. Devoret *et al.*, in *Quantum Tunneling in Condensed Media*, Y. Kagan, A. J. Leggett, Eds. (Elsevier Science, Amsterdam, 1992).
10. Y. Nakamura, Yu. A. Pashkin, J. S. Tsai, *Nature* **398**, 786, (1999).
11. C. H. van der Wal *et al.*, *Science* **290**, 773 (2000).
12. S. Han, R. Rouse, J. E. Lukens, *Phys. Rev. Lett.* **84**, 1300 (2000).
13. S. Han, Y. Yu, X. Chu, S. -I. Chu, Z. Wang, *Science* **293**, 1457 (2001).
14. J. M. Martinis, S. Nan, J. Aumentado, and C. Urbina (unpublished data) have recently obtained $Q_\varphi$'s reaching 1000 for a current-biased Josephson junction.
15. Y. Nakamura, Yu. A. Pashkin, T. Yamamoto, J. S. Tsai, *Phys. Rev. Lett.* **88**, 047901 (2002).
16. V. Bouchiat, D. Vion, P. Joyez, D. Esteve, M. H. Devoret, *Phys. Scr.* **T76**, 165 (1998).
17. A. Cottet *et al.*, *Physica C* **367**, 197 (2002).
18. Another two-port design has been proposed by A. B. Zorin [*Physica C* **368**, 284 (2002)].
19. M. T. Tuominen, J. M. Hergenrother, T. S. Tighe, M. Tinkham, *Phys. Rev. Lett.* **69**, 1997 (1992).
20. P. Lafarge, P. Joyez, D. Esteve, C. Urbina, M. H. Devoret, *Nature* **365**, 422 (1993).
21. D. V. Averin, K. K. Likharev, in *Mesoscopic Phenomena in Solids*, B. L. Altshuler, P. A. Lee, R. A. Webb, Eds. (Elsevier, Amsterdam, 1991).
22. J. R. Friedman, D. V. Averin, *Phys. Rev. Lett.* **88**, 50403 (2002).
23. A. Aassime, G. Johansson, G. Wendin, R. J. Schoelkopf, P. Delsing, *Phys. Rev. Lett.* **86**, 3376 (2001).
24. A different Cooper pair box readout scheme using a large Josephson junction is discussed by F. W. J. Hekking, O. Buisson, F. Balestro, and M. G. Vergniory, in *Electronic Correlations: From Meso- to Nanophysics*, T. Martin, G. Montambaux, J. Trân Thanh Vân, Eds. (Editions De Physique, Les Ulis, France, 2001), pp. 515–520.
25. For $C = 1$ pF and $I_0 = 0.77$ μA, the bare plasma frequency of the large junction is $\omega_p/2\pi \cong 8$ GHz, well below $\nu_{01}$.
26. A. Cottet *et al.*, in *Macroscopic Quantum Coherence and Quantum Computing*, D. V. Averin, B. Ruggiero, P. Silvestrini, Eds. (Kluwer Academic, Plenum, New York, 2001), pp. 111–125.
27. I. I. Rabi, *Phys. Rev.* **51**, 652 (1937).
28. N. F. Ramsey, *Phys. Rev.* **78**, 695 (1950).
29. In practice, the rotation axis does not need to be $x$, but the rotation angle of the two pulses is always adjusted so as to bring a spin initially along $z$ into the plane perpendicular to $z$.
30. At fixed $\Delta t$, the switching probability displays a decaying oscillation as a function of detuning.
31. H. Wolf *et al.*, *IEEE Trans. Instrum. Meas.* **46**, 303 (1997).
32. F. C. Wellstood, C. Urbina, J. Clarke, *Appl. Phys. Lett.* **50**, 772 (1987).



33. The indispensable technical work of P. Orfila is gratefully acknowledged. This work has greatly benefited from direct inputs from J. M. Martinis and Y. Nakamura. The authors acknowledge discussions with P. Delsing, G. Falci, D. Haviland, H. Mooij, R. Schoelkopf, G. Schön, and G. Wendin. Partly supported by the European Union through contract IST-10673 SQUBIT and the Conseil Général de l'Essone through the EQUM project.

26 December 2001; accepted 20 March 2002


# Coherent Temporal Oscillations of Macroscopic Quantum States in a Josephson Junction


**Yang Yu,[1] Siyuan Han,[1]* Xi Chu,[2]† Shih-I Chu,[2] Zhen Wang[3]**



**We report the generation and observation of coherent temporal oscillations between the macroscopic quantum states of a Josephson tunnel junction by applying microwaves with frequencies close to the level separation. Coherent temporal oscillations of excited state populations were observed by monitoring the junction's tunneling probability as a function of time. From the data, the lower limit of phase decoherence time was estimated to be about 5 microseconds.**


The question of whether macroscopic variables obey quantum mechanics has stimulated extensive theoretical interests (*1*, *2*). The experimental search for macroscopic quantum phenomena (MQP) did not start until the early 1980s, when theory showed that the experimental conditions for observing MQP in Josephson junction–based devices were achievable (*3*–*5*). Many MQP, such as macroscopic quantum tunneling (MQT) (*6*–*10*), energy level quantization (*11*, *12*), quantum incoherent relaxation (*13*), resonant tunneling and photon-assisted tunneling (*14*), and photo-induced transition and population inversion between macroscopic quantum states (*15*, *16*), have since been observed. Recent spectroscopy evidence of superposition of fluxoid states and persistent-current states in superconducting quantum interference devices has also been reported (*17*, *18*). However, time domain coherent oscillations between macroscopic quantum states (MQS), which is more direct evidence for the superposition of MQS, has thus far evaded experimental detection.

One of the methods proposed to create coherent temporal oscillations between two MQS is via Rabi oscillation, an effect that is well established and understood in atomic and molecular systems (*19*). The principle of Rabi oscillations is that by applying a monochromatic electromagnetic (EM) field to a quantum two-level system, which interacts with the EM fields, the system will be in a superposition of the two energy eigenstates that results in oscillations between the lower and upper levels with Rabi frequency $\Omega$. The amplitude of the population oscillations is at a maximum when the frequency of the EM wave $\omega$ is in resonance with the level spacing $\Delta E$, i.e., $\omega = \Delta E/\hbar$. Rabi oscillation is a coherent quantum phenomenon that provides the foundation to a wide variety of basic research and applications, ranging from coherent excitation of atoms and molecules by laser to quantum computation (*20*–*22*). Re-


[1]Department of Physics and Astronomy, [2]Department of Chemistry, University of Kansas, Lawrence, KS 66045, USA. [3]Kansai Advanced Research Center, Communication Research Laboratory, Ministry of Posts and Telecommunications, 588-2 Iwaoka, Iwaoka-cho, Nishi-ku, Kobe, 651-24 Japan.

*To whom correspondence and requests should be addressed. E-mail: han@ku.edu

†Present address: Institute for Theoretical Atomic and Molecular Physics, Harvard-Smithsonian Center for Astrophysics, 60 Garden Street, Cambridge, MA 02138, USA.

cently, Rabi oscillations have been observed in mesoscopic systems such as quantum dots and wells and single Cooper pair tunneling devices (*23*–*27*). We report experimental evidence for Rabi oscillations in a macroscopic quantum system, a Josephson junction (JJ).

In order to observe Rabi oscillations in a macroscopic quantum system, the decoherence time $\tau_d$ must be significantly greater than the period of Rabi oscillations. This requirement is readily satisfied in atomic and molecular systems but is very difficult to meet in macroscopic systems, such as Josephson junctions, because of the coupling that occurs between the macroscopic variables and the environmental degrees of freedom. Using a Josephson tunnel junction that is carefully shielded from noises and weakly coupled to its environment, we were able to generate and detect Rabi oscillations between the MQS of the junction. The result is a clear demonstration of the superposition of macroscopic quantum states, a necessary requirement for the realization of pulse-driven superconducting quantum gates (*20*, *22*).

The dynamics of a JJ is equivalent to that of a fictitious particle of mass $C$ moving in a washboard potential $U(\Phi) = -I_b\Phi - E_J\cos(2\pi\Phi/\Phi_0)$, where $C$ is the junction capacitance, $\Phi_0 \equiv h/2e$ is the flux quantum, $E_J \equiv I_c\Phi_0/2\pi$ is the magnitude of maximum Josephson coupling energy, $I_c$ is the critical current of the junction, $I_b$ is the bias current, and $\Phi \equiv (\delta/2\pi)\Phi_0$ (where $\delta$ is the gauge-invariant phase difference of the superconducting order parameter across the junction) (*28*). An underdamped JJ with $I_b < I_c$ has two distinctive voltage states: The zero-voltage state corresponds to the particle being trapped in a metastable potential well, and the finite voltage state corresponds to the particle running down the washboard potential. It is also well established that underdamped JJ's have quantized energy levels and that microwaves can excite transitions between these levels (*9*, *11*, *12*). For a JJ pumped by microwaves, Rabi oscillations are expected to occur for $\tau_d \gg 2\pi/\Omega$. In the opposite limit of $\tau_d \ll 2\pi/\Omega$, the dynamics is incoherent and no coherent oscillations will occur.

Being able to generate Rabi oscillations in a JJ is not sufficient for their observation. In addition, one must also be able to detect them. We used the tunneling rate from the potential well to probe population $\rho_{11}$ of the upper level $|1\rangle$. Because the tunneling rate from level $|1\rangle$ is more than $10^3$ times that from level $|0\rangle$, the total tunneling rate is strongly influenced by $\rho_{11}$. In addition to tunneling, there are also the processes of interlevel decay and dephasing that affect the dynamics of the junction. The situation is depicted in Fig. 1, where $\Gamma_i$ denotes the tunneling rate from level $|i = 0, 1\rangle$ and $\gamma_{10}$ denotes the rate of energy relaxation from $|1\rangle$ to $|0\rangle$. Because the tunneling rates depend exponentially on the barrier height, the bias currents can be chosen so that the tunneling from $|0\rangle$ is essentially "frozen out" and escapes are mostly from the upper levels. Therefore, the time-dependent tunneling probability probes the temporal variation of the upper level population directly.

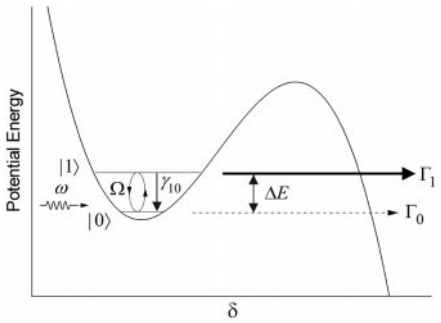


**Fig. 1.** An illustration of various coherent and incoherent processes in a metastable quantum two-level system radiated by a microwave. The model is applicable to a Josephson junction radiated by a monochromatic microwave.

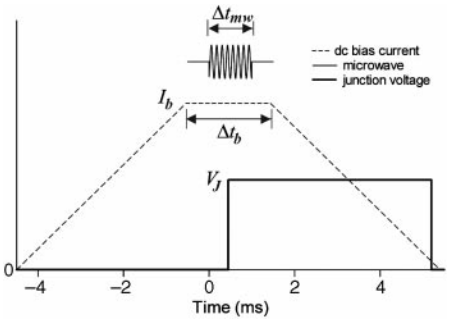


**Fig. 2.** An illustration of the timing of the dc current bias, microwave, and junction voltage. The junction's average lifetime in the zero-voltage state is much shorter than the microwave pulse duration, $\Delta t_{mw}$.

In the rotating wave approximation, the quantum dynamics of a Josephson junction with microwave excitations, including the effects of various decaying rates (Fig. 1), is described by the Liouville equation of the time evolution of the density matrix operator

$$\frac{du}{dt} = \Delta v(t) - \Gamma u(t), \quad (1)$$

$$\frac{dv}{dt} = -\Delta u(t) - \Gamma v(t) + \Omega_0 w(t), \quad (2)$$

$$\frac{dw}{dt} = -\frac{1}{2}(\Gamma_1 + 2\gamma_{10} + \Gamma_0)w(t) - \Omega_0 v(t) - \frac{1}{2}(\Gamma_1 + 2\gamma_{10} - \Gamma_0)S(t), \quad (3)$$

$$\frac{dS}{dt} = -\frac{1}{2}(\Gamma_1 + \Gamma_0)S(t) - \frac{1}{2}(\Gamma_1 - \Gamma_0)w(t) \quad (4)$$

where $\Delta = (E_1 - E_0)/\hbar - \omega$ is the detuning (with $\omega$ the microwave frequency), $\Omega_0 = |\delta_{01} i_{rf} E_J/\hbar|$ is the on-resonance ($\Delta = 0$) Rabi frequency, $i_{rf}$ is the amplitude of microwave current normalized to $I_c$, $\delta_{01} = \langle 0|\delta|1\rangle$ is the coupling matrix element, $u = \rho_{01} + \rho_{10}$, $v = \frac{1}{i}(\rho_{01} - \rho_{10})$, $w = \rho_{11} - \rho_{00}$, and $S = \rho_{11} + \rho_{00}$. In addition, we have defined $\Omega \equiv \sqrt{\Omega_0^2 - (\Gamma - i\Delta)^2}$ as the Rabi frequency and $\Gamma$ as the total off-diagonal decay rate given by $\Gamma = \frac{1}{2}(\Gamma_1 + \Gamma_0 + \gamma_{10}) + \gamma_\varphi$ (with $\gamma_\varphi$ as the dephasing rate). The set of Liouville equations can be solved analytically by means of the Laplace transformation technique, from which the time-dependent populations of both levels can be obtained. The exact analytical solutions are too cumbersome to present here. However, in the limit of $\Gamma_1 > \gamma_{10} > \gamma_\varphi > \Gamma_0$, a situation likely to be applicable here, we obtain the approximate analytical solution as follows

$$\rho_{11}(t) = e^{-\Gamma t}\frac{\Omega_0^2}{|\Omega^2|}\left|\sin\left(\frac{\Omega t}{2}\right)\right|^2 \quad (5)$$

which describes damped oscillations, in contrast to the simple exponential decay behavior of incoherent processes.

We used a 10 μm by 10 μm NbN/AlN/NbN junction. The junction parameters, $I_c \simeq 147.9$ μA and $C = 5.8 \pm 0.6$ pF, were obtained from independent measurements in the thermal regime. $I_c$ and $C$, together with $I_b$, uniquely determine the energy level separations. All electrical leads connected to the junction are carefully filtered. The measured switching current distributions of junctions on the same chip but with much smaller critical current were consistent with the prediction of MQT theory to $T = 8$ mK, indicating that the effect of extrinsic noises was negligible. A more detailed description of our experimental setup can be found elsewhere (*29*). Because the junction was inside a high Q (high quality factor) cavity, it was difficult to sweep the microwave frequency while keeping constant the power coupled to the junction. Therefore, varying detuning parameter $\Delta$ was accomplished by changing the junction's dc bias current $i_b \equiv I_b/I_c$ (thus the level separation) while keeping $\omega$ constant. Another important property of the system is that the tunneling rate is sensitive to the applied microwave power. If the power is too high, it will cause significant strong field effects (e.g., multiphoton transitions). Conversely, weaker microwave power results in smaller amplitude of Rabi oscillations due to the finite detuning.

The measurement of the time evolution of

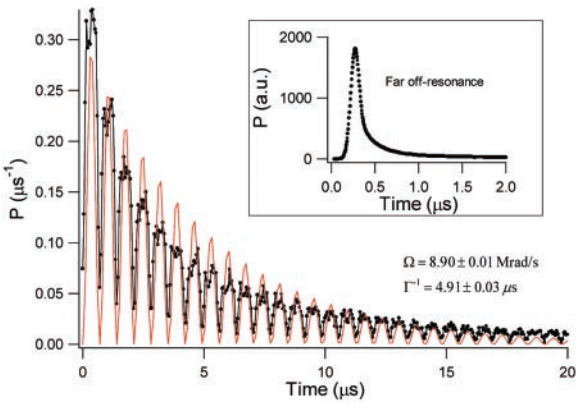


**Fig. 3**. Tunneling probability density $P(t)$ measured at 8 mK at $i_b \simeq 0.993$ with the microwave frequency set to $f = 16.500$ GHz. The frequency detuning $\Delta$ is estimated to be less than 5 Mrad/s, and the on-resonance Rabi frequency is $\sim\Delta$. The circles (connected by the black line to guide eyes) are data and the solid line is the best fit to Eq. 5. (Inset) Data taken at a slightly higher dc bias current where the detuning value is much larger.

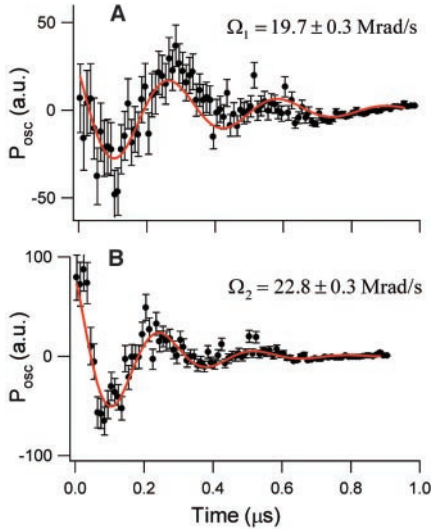


**Fig. 4.** Microwave power dependence of Rabi frequency with (**A**) 7.8 pW and (**B**) 10 pW injected to the sample cell. The circles are data and the red solid lines are the best fit to the oscillatory part of Eq. 6. The higher bias current $i_b \simeq 0.994$ results in a faster exponential decay (see Eq. 5).

tunneling probability density $P(t)$ is as follows: for each measurement cycle, the junction's bias current was ramped up to and kept at $I_b$ for a period of $\Delta t_b$ (Fig. 2). At this bias level, typically around $i_b \gtrsim 0.99$, the average time remaining in the zero-voltage state without microwave is much greater than $\Delta t_b$ so that almost no escape would occur at $t < \Delta t_b$. A microwave pulse of frequency $f = \omega/2\pi$ and duration $\Delta t_{mw}$ was then applied (Fig. 2) to the junction via a cryogenic semirigid coaxial cable, which generates oscillations in upper-level population and thus a periodic enhancement of the tunneling rate. The time at which the junction switched from the zero to finite voltage state, the escape time, was recorded using a timer with subnanosecond resolution. The process was repeated $10^4$ to $10^5$ times. The tunneling probability density $P(t)$, the number of tunneling events per unit time, was then obtained from the histogram of escape times. $P(t)$ is approximately proportional to $\rho_{11}$ for $\Gamma_0 \ll \Gamma_1$. With the limit of $\Delta = 0$ and fast decay, Eq. 5 becomes

$$\rho_{11}(t) = e^{-\Gamma t}\frac{\Omega_0^2}{2|\Omega^2|}(1-\cos\Omega t) \qquad (6)$$

In Fig. 3, the measured tunneling probability density is shown as a function of time. The frequency and duration of the microwave pulses are $\omega/2\pi = 16.5$ GHz and $\Delta t_{mw} = 0.1$ ms. Because all tunneling events occurred at $t < \Delta t_{mw}$, the effect of microwave pulse is the same as that of a continuous wave turned on at $t = 0$. The measured $P(t)$ clearly shows the damped temporal oscillations described by Eq. 5. The peaks and dips in $P(t)$ correspond to the population of excited state reaching maxima and minima, respectively. The period of oscillations and the decay time, obtained from fitting the data to Eq. 5, are $\Omega = 8.90 \pm 0.01$ megarad/s and $\Gamma^{-1} = 4.91 \pm 0.03$ μs. However, observation of damped $P(t)$ oscillations is necessary but not sufficient evidence of Rabi oscillation because the oscillations can also be due to other mechanisms. For instance, the observed oscillations could be caused by frequency beats between the applied microwave and a cavity mode, which would lead to $P(t)$ oscillations with frequency $\Delta\omega \equiv \omega - \omega_{cav}$, where $\omega_{cav}$ is the frequency of the cavity mode. In this case $P(t)$ would not be sensitive to variations in detuning $\Delta$ when $\Delta\omega$ was fixed. In contrast, for weak microwave fields, the amplitude of $P(t)$ oscillations due to Rabi mechanism depends strongly on the detuning $\Delta$. Therefore, the $\Delta$ dependence of $P(t)$ can be used to verify whether the observed oscillations were due to the cavity-microwave interaction. To do this, $P(t)$ was measured at a slightly higher bias current $i_b$ while keeping all other parameters the same. There are two major effects of increasing $i_b$. One of them is to reduce the level spacing, thus increasing the detuning $\Delta$; the other is to increase the tunneling rate so that the total off-diagonal decay rate $\Gamma$ would be much greater. The inset of Fig. 3 shows what happened when the dc bias current was increased by a very small amount of $\delta i_b \lesssim 2 \times 10^{-3}$. It can be seen that oscillations in $P(t)$ were washed out and the overall tunneling rate was much higher. The observed $\Delta$ dependence is, therefore, inconsistent with the cavity-microwave interaction mechanism.

In the limit of small detuning $\Delta \ll \Omega$, Eq. 5 predicts that the frequency of $\rho_{11}$ oscillations, and hence the tunneling probability, is proportional to the amplitude of the microwave. Therefore, when the amplitude of the microwave is changed from $A_1$ to $A_2$, the frequency of Rabi oscillations should vary in accordance with $\Omega_1/\Omega_2 \simeq A_1/A_2$. The relation provides a very useful test for Rabi oscillations in the Josephson junction. Although the absolute values of microwave amplitude coupled to the junction could not be determined by our experiment, the ratio $A_1/A_2$ was precisely determined. Figure 4 shows the oscillatory part of the excited state population $P_{osc}$ as a function of time with two different microwave power levels. The data were taken at $i_b \simeq 0.994$, $\omega/2\pi = 16.000$ GHz, and with $A_1/A_2 = 0.88$. As microwave power was increased the angular frequency of the oscillations, obtained from the best fits, increased from $\Omega_1 = 19.7 \pm 0.3$ megarad/s to $\Omega_2 = 22.8 \pm 0.3$ megarad/s. The ratio $\Omega_1/\Omega_2 = 0.864 \pm 0.025$ is in good agreement with the theory. Therefore, we conclude that the observed oscillations were due to microwave excited coherent Rabi oscillations between the macroscopic quantum states of the JJ.

Our result demonstrates the coherent superposition and temporal oscillations of macroscopic quantum states in a JJ, which has important implications for quantum state engineering of Josephson devices and quantum computation with the use of superconducting qubits. For instance, one of the most important properties of these qubits is the phase decoherence time $\tau_\varphi \equiv \gamma_\varphi^{-1}$, which sets the time scale over which phase coherence can be maintained. In our experiment, the decay time constant $\tau = \Gamma^{-1}$ sets a lower limit for $\tau_\varphi$ because $\Gamma$ is always greater than $\gamma_\varphi$. From the data (Fig. 3), we estimated that the phase decoherence time is greater than 4.9 μs, which is consistent with the previous result of post-pulse escape rate measurements (*29*). Lastly, being able to generate Rabi oscillations in Josephson junctions greatly enhances the prospects of realizing quantum computation with microwave pulse-driven superconducting qubits (*20–22*).

### References and Notes

1. E. Schrödinger, *Naturwissenschaften* **23**, 844 (1935).
2. A. J. Leggett, A. Garg, *Phys. Rev. Lett.* **54**, 857 (1985).
3. A. O. Caldeira, A. J. Leggett, *Phys. Rev. Lett.* **46**, 211 (1981).
4. A. J. Leggett, *Quantum Tunneling in Condensed Media*, vol. 34 of *Modern Problems in Condensed Matter Sciences*, Y. Kagan, A. J. Leggett, Eds. (North-Holland, Amsterdam, 1992) chap. 1, pp. 1–36.
5. A. J. Leggett *et al., Rev. Mod. Phys.* **59**, 1 (1987).

6. R. F. Voss, R. A. Webb, *Phys. Rev. Lett.* **47**, 265 (1981).
7. S. Washburn, R. A. Webb, R. F. Voss, S. M. Faris, *Phys. Rev. Lett.* **54**, 2712 (1985).
8. D. B. Schwartz, B. Sen, C. N. Archie, J. E. Lukens, *Phys. Rev. Lett.* **55**, 1547 (1985).
9. J. Clarke, A. N. Cleland, M. H. Devoret, D. Esteve, J. M. Martinis, *Science* **239**, 992 (1988).
10. M. H. Devoret, J. M. Martinis, J. Clarke, *Phys. Rev. Lett.* **55**, 1908 (1985).
11. J. M. Martinis, M. H. Devoret, J. Clarke, *Phys. Rev. Lett.* **55**, 1543 (1985).
12. P. Silvestrini, V. G. Palmieri, B. Ruggiero, M. Russo, *Phys. Rev. Lett.* **79**, 3046 (1997).
13. S. Han, J. Lapointe, J. E. Lukens, *Phys. Rev. Lett.* **66**, 810 (1991).
14. R. Rouse, S. Han, J. E. Lukens, *Phys. Rev. Lett.* **75**, 1614 (1995).
15. S. Han, R. Rouse, J. E. Lukens, *Phys. Rev. Lett.* **76**, 3404 (1996).
16. ———, *Phys. Rev. Lett.* **84**, 1300 (2000).
17. J. R. Friedman, V. Patel, W. Chen, S. K. Tolpygo, J. E. Lukens, *Nature* **406**, 43 (2000).
18. C. H. van der Wal *et al.*, *Science* **290**, 773 (2000).
19. I. I. Rabi, *Phys. Rev.* **51**, 652 (1937).
20. S. Lloyd, *Science* **261**, 1569 (1993).
21. M. F. Bocko, A. M. Herr, M. J. Feldman, *IEEE Trans. Appl. Supercond.* **7**, 3638 (1997).
22. Y. Makhlin, G. Schön, A. Shnirman, *Rev. Mod. Phys.* **73**, 357 (2001).
23. T. H. Stievater *et al.*, *Phys. Rev. Lett.* **87**, 133603 (2001).
24. R. H. Blick, D. W. van der Weide, R. J. Haug, K. Eberl, *Phys. Rev. Lett.* **81**, 689 (1998).
25. C. A. Stafford, N. S. Wingreen, *Phys. Rev. Lett.* **76**, 1916 (1996).
26. A. Schülzgen *et al.*, *Phys. Rev. Lett.* **82**, 2346 (1999).
27. Y. Nakamura, Y. A. Pashkin, J. S. Tsai, *Phys. Rev. Lett.* **87**, 246601 (2001).
28. A. Barone and G. Paterno, *Physics and Applications of the Josephson Effect* (John Wiley and Sons, New York, 1982) pp. 1–14.
29. S. Han, Y. Yu, X. Chu, S. Chu, Z. Wang, *Science* **293**, 1457 (2001).


30. We thank Y. Zhang and S. Li for technical assistance in preparing the experiment. S.H. thanks J. E. Lukens for useful discussions. Supported in part by NSF (DMR-9876874 and EIA-0082499) and by Air Force Office of Scientific Research (AFOSR) (grant F49620-01-1-0439), funded under the Department of Defense University Research Initiative on Nanotechnology (DURINT) program and by the Advanced Research and Development Activity (ARDA).

2 January 2002; accepted 15 March 2002


# Ordering of Quantum Dots Using Genetically Engineered Viruses


**Seung-Wuk Lee, Chuanbin Mao, Christine E. Flynn, Angela M. Belcher*†**



**A liquid crystal system was used for the fabrication of a highly ordered composite material from genetically engineered M13 bacteriophage and zinc sulfide (ZnS) nanocrystals. The bacteriophage, which formed the basis of the self-ordering system, were selected to have a specific recognition moiety for ZnS crystal surfaces. The bacteriophage were coupled with ZnS solution precursors and spontaneously evolved a self-supporting hybrid film material that was ordered at the nanoscale and at the micrometer scale into ~72-micrometer domains, which were continuous over a centimeter length scale. In addition, suspensions were prepared in which the lyotropic liquid crystalline phase behavior of the hybrid material was controlled by solvent concentration and by the use of a magnetic field.**


Building ordered and defect-free two- and three-dimensional structures on the nanometer scale is essential for the construction of next-generation optical, electronic, and magnetic materials and devices (*1–4*). Traditional assembly approaches have been based on hydrogen bonding, coulombic interactions, and van der Waals forces (*1, 4*). Although a bacterial synthetic method was reported to make monodisperse modified polypeptides (*5*), it has been difficult to tune the layer spacing and structure of conventional synthetic polymers because of their polydisperse chain lengths (*6*). Efforts have been directed toward the use of soft materials to organize inorganic materials at the nanoscale. Protein cages have been used as templates to synthesize nanoscale materials in capsids (*7*). DNA recognition linkers have been successfully used to construct specific gold nanocrystal structures (*8, 9*). ZnS and CdS were nucleated in a lyotropic liquid crystalline medium to make nanowires and nanocrystal superlattice structures by a surfactant assembly pathway (*10*). However, these methods have limitations with respect to length scale and type of inorganic material.

Monodisperse biomaterials that have an anisotropic shape are promising as components of well-ordered structures. Liquid crystalline structures of wild-type viruses (Fd, M13, and TMV) were tunable by controlling the solution concentrations, the solution ionic strength, and the external magnetic fields applied to the solutions (*11–14*). We recently showed that engineered viruses can recognize specific semiconductor surfaces through the method of selection by combinatorial phage display (*15*). These specific recognition properties of the virus can be used to organize inorganic nanocrystals, forming ordered arrays over the length scale defined by liquid crystal formation. We have evolved phage and ZnS precursor solutions to self-assemble highly oriented, self-supporting films. In this system, we can easily modulate both the length of bacteriophage and the type of inorganic materials through genetic modification and selection. Here we report our first effort to direct multi–length scale ordering of quantum dot (QD) hybrid self-supporting biocomposite structures using genetically engineered M13 bacteriophage, viruses with monodisperse size and shape. The resulting QD hybrid film material was ordered at the nanoscale and at the micrometer scale into 72-μm domains. These domains repeated continuously over a centimeter length scale. Moreover, viral suspensions containing ZnS QDs were prepared in which the liquid crystalline phase behaviors of the hybrid material were controlled by solvent concentration and by the use of an applied magnetic field.

The most dominant selected peptide binding motif with specific recognition of ZnS crystal surfaces was isolated through screening of phage display libraries (Fig. 1) (*16, 17*). The screening method selected for binding affinity of a population of random peptides displayed as part of the pIII minor coat protein of M13. Selected peptides were expressed at one end of the M13 virus. The virus had a filamentous shape (~880 nm in length and 6.6 nm in diameter), with the peptide insert measuring 10 nm in length (*11*). The dominant binding motif that emerged after five rounds of selection was termed A7, with an amino acid insert sequence (Cys-Asn-Asn-Pro-Met-His-Gln-Asn-Cys) in which the two cysteine groups formed a disulfide bond, restricting the peptide structure to a constrained loop (*16*). The peptide expressed on the virus was tested and confirmed to have binding specificity to ZnS crystal surfaces (*16, 18*). The bacteriophage containing this A7 peptide—termed A7 phage—was cloned and amplified to liquid crystalline concentrations, with DNA verification after each amplification step.

The A7 phage was precipitated and then resuspended in ZnS precursor solutions to form an A7 phage–ZnS nanocrystal (A7-ZnS) liquid crystalline suspension (*19*). The liquid crystalline behavior of the suspensions was dominated by the long-rod phage shape, despite the at-


Department of Chemistry and Biochemistry, Center for Nano- and Molecular Science and Technology, Texas Materials Institute, Institute for Cellular and Molecular Biology, University of Texas at Austin, Austin, TX 78712, USA.

*Present address: Department of Materials Science and Engineering and Biological Engineering, Massachusetts Institute of Technology, Cambridge, MA 02139, USA.

†To whom correspondence should be addressed. E-mail: belcher@mit.edu